Optics Letters

# Noise analysis of speckle-based x-ray phase-contrast imaging

Tunhe Zhou,[1,*] Marie-Christine Zdora,[2,3] Irene Zanette,[2] Jenny Romell,[1] Hans M. Hertz,[1] and Anna Burvall[1]

[1]Biomedical and X-Ray Physics, KTH Royal Institute of Technology, 10691 Stockholm, Sweden
[2]Diamond Light Source, Harwell Science and Innovation Campus, Didcot, Oxfordshire OX11 0DE, UK
[3]Department of Physics and Astronomy, University College London, London WC1E 6BT, UK
*Corresponding author: tunhe@kth.se

Received 3 August 2016; revised 30 October 2016; accepted 30 October 2016; posted 1 November 2016 (Doc. ID 270193); published 22 November 2016

**Speckle-based x-ray phase-contrast imaging has drawn increasing interest in recent years as a simple, multimodal, cost-efficient, and laboratory-source adaptable method. We investigate its noise properties to help further optimization on the method and further comparison with other phase-contrast methods. An analytical model for assessing noise in a differential phase signal is adapted from studies on the digital image correlation technique in experimental mechanics and is supported by simulations and experiments. The model indicates that the noise of the differential phase signal from speckle-based imaging has a behavior similar to that of the grating-based method.** 

***OCIS codes:*** (110.6150) Speckle imaging; (110.7440) X-ray imaging; (110.4280) Noise in imaging systems.

https://doi.org/10.1364/OL.41.005490

X-ray phase-contrast imaging (XPCI) has received much interest due to its better sensitivity for materials with low atomic numbers in the hard x-ray domain, compared to traditional absorption contrast imaging. Different XPCI methods have been developed, among which speckle-based imaging (SBI) has drawn increased attention in recent years [1,2] for its flexibility in an experimental arrangement, cost efficiency, and good adaptability to laboratory systems.

The principle of SBI is to use a static diffuser to generate a near-field speckle pattern [3] on the detector as a wavefront marker. By tracking the change of the speckle pattern induced by an object, including attenuation in intensity, local shift of the patterns, and loss of local visibility, we can simultaneously acquire transmission, differential phase-contrast (DPC) and dark-field images.

Different SBI techniques have been developed, namely single-shot speckle tracking (ST) [1,2] and several versions of speckle scanning [4,5]. The first one is intuitive, as the tracking is applied directly on two images, with and without an object. The speckle-scanning technique is principally similar to the grating-based imaging method (GBI) [6,7]: the diffuser is scanned either in one direction [5] or on a 2D grid [8]. The retrieval process is applied on the intensity variance maps formed from all the scan steps for each pixel.

For GBI, the error propagation from original images to the phase derivative is known [9,10]. SBI, where the phase derivative must be reconstructed from numerical optimization, has not yet been explored. A quantitative expression for the noise property of SBI will allow a better understanding and further optimization of the method. This Letter mainly discusses the single-shot speckle-tracking technique, as it is simplest and commonly used.

An object in an x-ray beam induces a phase shift $\phi$ to the propagating wave and causes the x-rays to refract. The angle $\alpha$, by which the exiting wave deviates from the incident wave, is proportional to the derivative of the phase shift as $\alpha \approx \frac{\lambda}{2\pi}\frac{\partial\phi(x)}{\partial x}$ when $\alpha$ is small, where $\lambda$ is the wavelength of the x-rays. If there is a wavefront marker, such as the near-field speckle pattern in SBI, $\alpha$ will lead to a transverse local shift $s$ of the pattern related to the propagation distance $d$ as

$$s = \frac{\lambda}{2\pi}\frac{\partial\phi(x)}{\partial x}d, \tag{1}$$

as illustrated in Fig. 1(a). When discussing noise in DPC, we therefore discuss the noise in the estimated local displacement $\hat{s}$.

One common reconstruction method for ST is to model the sample image as $\hat{I}(\boldsymbol{r}) = T(\boldsymbol{r}+\hat{\boldsymbol{s}})I_0(\boldsymbol{r}+\hat{\boldsymbol{s}})$, where $T$ is the transmission and $I_0$ is the measured speckle image without an object (named as reference image) [11]. The dark-field signal is not included in this model as we assume the object has low scattering strength. $T$ and $\hat{\boldsymbol{s}}$; can then be retrieved by finding the least-square difference between the model $\hat{I}$ and the measured sample image $I$ as

$$\chi^2 = w * [\hat{I} - I]^2 = \int w(\boldsymbol{r_0}-\boldsymbol{r})\cdot[\hat{I}(\boldsymbol{r}) - I(\boldsymbol{r})]^2 \mathrm{d}^2 r, \tag{2}$$

where $w$ is a window function to choose a subset for this correlation process, and $*$ is the convolution operator. In this Letter, a rectangular window is always used for simplicity;

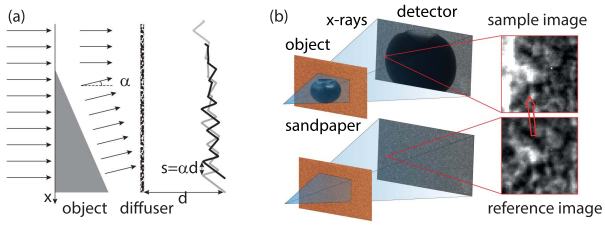


**Fig. 1.** (a) Simplified illustration of an object inducing phase shift to the propagating wave, which converts into a refraction angle and leads to a transverse displacement on the detected image. (b) Speckle-tracking method experiment arrangement. A correlation analysis is done on a small window of subsets extracted from the images taken with and without samples.

hence, the integration can be seen as a sum over all the pixels within the rectangular window directly.

Although x-ray SBI has only been developed for a few years, techniques using pattern matching with similar principles have been widely applied in different areas. For example, in experimental mechanics, the photos of speckle-like patterns are used for measuring stress or motion [12] and, in the fields of cardiology and medical imaging, speckle-tracking echocardiography is used to analyze the motion of tissues or blood [13]. An experimental and theoretical analysis has been done on the errors of digital image correlation in the field of mechanics [14,15]. Here we derive an analytical model for DPC noise in an x-ray SBI based on an established model from the study of the digital image correlation [16,17].

As our main interest is in the phase, we assume $T = 1$. Defining the difference between the estimate of the local shift and the expected value as the error $\boldsymbol{e} = \hat{\boldsymbol{s}} - \boldsymbol{s}$, we find

$$\begin{aligned}\hat{I}(\boldsymbol{r}) &= I_0(\boldsymbol{r}+\boldsymbol{s}+\boldsymbol{e}) \simeq I_0(\boldsymbol{r}+\boldsymbol{s}) + \nabla I_0(\boldsymbol{r}+\boldsymbol{s})\cdot\boldsymbol{e} \\ &= I(\boldsymbol{r}) + \nabla I(\boldsymbol{r})\cdot\boldsymbol{e} \\ &= I(\boldsymbol{r}) + [g_x(\boldsymbol{r}) \quad g_y(\boldsymbol{r})]\cdot[e_x \quad e_y]^{\mathrm{tr}}, \end{aligned} \tag{3}$$

where $g_x(\boldsymbol{r}) = \partial I(\boldsymbol{r})/\partial x$, $g_y(\boldsymbol{r}) = \partial I(\boldsymbol{r})/\partial y$, and tr denotes transpose of the matrix. The error $\boldsymbol{e}$ is assumed small enough that the higher-order terms in the Taylor expansion can be ignored. The model assumes perfect sampling; hence, $I_0(\boldsymbol{r}+\boldsymbol{s}) = I(\boldsymbol{r})$. If not, different interpolation algorithms need to be discussed, which is not included here. Some examples have been derived in [16] and show that when interpolation is employed the reconstruction is biased, but the variance remains the same.

Substituting Eq. (3) into Eq. (2), and including the noise $\varepsilon_0$ and $\varepsilon$ present in the reference and sample images under the assumption of white Gaussian photon noise, we have

$$\begin{aligned}\chi^2 &= \int w(\boldsymbol{r}_0-\boldsymbol{r})\cdot[\hat{I}(\boldsymbol{r}) + \varepsilon_0(\boldsymbol{r}+\hat{\boldsymbol{s}}) - I(\boldsymbol{r}) - \varepsilon(\boldsymbol{r})]^2 \mathrm{d}^2 r \\ &= \int w(\boldsymbol{r}_0-\boldsymbol{r})\cdot[g_x(\boldsymbol{r})e_x + g_y(\boldsymbol{r})e_y + \varepsilon_0(\boldsymbol{r}+\hat{\boldsymbol{s}}) - \varepsilon(\boldsymbol{r})]^2 \mathrm{d}^2 r. \end{aligned}$$

Minimizing $\chi^2$ by solving $\frac{\partial \chi^2}{\partial e_i} = 0$, $i = x, y$, we get [16]

$$[e_x \quad e_y]^{\mathrm{tr}} = \begin{bmatrix} \int w g_x^2 \mathrm{d}^2 r & \int w g_x g_y \mathrm{d}^2 r \\ \int w g_x g_y \mathrm{d}^2 r & \int w g_y^2 \mathrm{d}^2 r \end{bmatrix}^{-1} \times \begin{bmatrix} \int w\varepsilon g_x \mathrm{d}^2 r - \int w\varepsilon_0 g_x \mathrm{d}^2 r \\ \int w\varepsilon g_y \mathrm{d}^2 r - \int w\varepsilon_0 g_y \mathrm{d}^2 r \end{bmatrix},$$

where the variables $\boldsymbol{r}_0$ and $\boldsymbol{r}$ are suppressed for simplicity, e.g., $w = w(\boldsymbol{r}_0 - \boldsymbol{r})$.

We assume stationary statistics for the speckle pattern. From here on, we only calculate the variance in the x-direction as representative for both directions [16]:

$$\begin{aligned}\sigma_{s_x}^2 &\approx 2\sigma_{\mathrm{ph}}^2 \frac{(\int w g_y^2 \mathrm{d}^2 r)^2 \int w^2 g_x^2 \mathrm{d}^2 r + (\int w g_x g_y \mathrm{d}^2 r)^2 \int w^2 g_y^2 \mathrm{d}^2 r}{[\int w g_y^2 \mathrm{d}^2 r \int w g_x^2 \mathrm{d}^2 r - (\int w g_x g_y \mathrm{d}^2 r)^2]^2} \\ &\approx \frac{2\sigma_{\mathrm{ph}}^2}{\int w g_x^2 \mathrm{d}^2 r}, \end{aligned} \tag{4}$$

where $\sigma_{\mathrm{ph}}^2$ is the variance of the photon noise, which is assumed to be uncorrelated and approximately the same for different pixels. The approximation is valid for the window functions of weight 1 (i.e., $w = 1$ within the window) and, under the assumption that for random speckle patterns and sufficiently large window sizes, the covariance of the gradients in the two directions within the subset window is null, i.e.,

$$\int w g_x g_y \mathrm{d}^2 r \approx 0. \tag{5}$$

From Eq. (1), it is also possible to get the variance for the differential phase as

$$\sigma_{\partial_x \phi}^2 = \left(\frac{2\pi}{\lambda d}\right)^2 \sigma_{s_x}^2 = \left(\frac{2\pi}{\lambda d}\right)^2 \frac{2\sigma_{\mathrm{ph}}^2}{\int w g_x^2 \mathrm{d}^2 r}.$$

This variance equation for SBI can be compared to the expression for the variance of GBI [9,10]:

$$\sigma_\varphi^2 = \frac{2\bar{\sigma}_{\mathrm{ph}}^2}{v^2 N \bar{I}^2}, \tag{6}$$

where $\varphi$ denotes the phase difference in the sinusoidal intensity function for GBI, $N$ is the number of phase-stepping steps, $v$ is the visibility, $\bar{\sigma}_{\mathrm{ph}}^2$ is the average of the photon noise for different phase-stepping positions, and $\bar{I}$ is the average intensity. Equations (4) and (6) are in similar forms: both are proportional to the photon noise with a scaling factor. The scaling factor for ST, $(\int w g_x^2 \mathrm{d}^2 r)^{-1}$, is related to the speckle-pattern visibility, in a manner similar to the GBI method. We define a concept related to the visibility for ST as $v_x = \sqrt{\frac{1}{N}\Sigma|\frac{\partial I}{\partial x}|^2}/\bar{I}$ with a physical meaning of normalized average gradient indicating the absolute contrast of the speckle pattern within the window, where $N$ is the total number of pixels within a window by using a rectangular function. Then Eq. (4) can be written as

$$\sigma_{s_x}^2 = \frac{2\sigma_{\mathrm{ph}}^2}{v_x^2 N \bar{I}^2}, \tag{7}$$

which is very similar to the expression for GBI, as $N$ in Eq. (6) can also be regarded as the number of data points in the correlation analysis.

The speckle-scanning technique shares the same principle as that of speckle tracking, except that $\int w g_x^2 \mathrm{d}^2 r$ needs to be taken from the scanned intensity map, and the window function is

normally chosen as 1 to use the whole size of the scanned map. If the scan step is much smaller than one effective pixel size, $g_x$ and $g_y$ in the scanned intensity map of one pixel are likely to be correlated; hence, Eq. (5) might not be valid.

Simulations are performed to support the analytical model using the Fresnel diffraction theory under the projection approximation [18] in a similar manner to [10,19]. Experiments are performed using a liquid-metal-jet source, a piece of sandpaper as a diffuser, and a CCD camera with a pixel size of 9 μm. The arrangement in both cases follows that of Fig. 1(b).

From Eq. (4), it follows that if $\int w g_x^2 \mathrm{d}^2 r$ is constant, $\sigma_{s_x}^2$ is linearly dependent on photon noise $\sigma_{\mathrm{ph}}^2$. This is difficult to verify experimentally since varying the exposure time to change $\sigma_{\mathrm{ph}}^2$ also alters $g_x$. In simulations, the variance of noise can be changed without altering the gradient $g_x$ by disconnecting the mean of the Gaussian distribution from its variance. Figure 2(a) shows the results of the simulations done as described above with $\sigma_{\mathrm{ph}}^2$ changed from zero to four times its original value. The window function $w$ is a 24 × 24 pixel 2D rectangular function. The source is assumed to be monochromatic with an energy of 16 keV to speed up the simulations. The diffuser is 1 m, and the detector is 2.9 m from the source. The variance of the simulated local shift for different $\sigma_{\mathrm{ph}}^2$ is marked as dots, with error bars from five repeated simulations with 1000 individually retrieved data points each. The noise predicted from Eq. (4) shown as a solid line agrees quite well with the simulated data. Some practical factors such as how the gradient of the image is calculated and the limitations of the assumptions that $\sigma_{\mathrm{ph}}^2$ is homogeneous in the image and that the higher-order terms can be omitted in the derivation of Eq. (3) can cause the deviations between the values from the analytical model and simulations.

Simulations are also undertaken with varied exposure times and the correct relation between mean and variance in the Gaussian distribution. The simulated results (circles) and predicted values (solid line) are shown in Fig. 2(b). As photon noise $\sigma_{\mathrm{ph}}^2 \propto I \propto t$, where $t$ is exposure time, and $\int w g_x^2 \mathrm{d}^2 r \propto t^2$, it can be deduced from Eq. (4) that $\sigma_{s_x}^2 \propto t^{-1}$. As quite long exposure times are applied for these simulations, the noise behavior from simulations agrees very well with the prediction, but we can still observe that at a relatively shorter exposure time (200 s), i.e., higher noise, the standard deviation of the simulated noise is larger than at longer exposure times.

Experiments are also done under varied exposure times, and the measured results (circles) are compared to the analytical model (solid line) in Fig. 3. The source was operated at 40 kVp with an emission current of 0.6 mA. The diffuser is a piece of P800 sandpaper placed 0.65 m after the source and 0.85 m before the detector. Images were acquired with

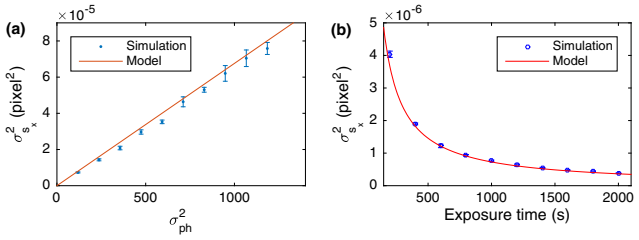


**Fig. 2.** (a) Simulations with a varied image noise variance, but the same intensity. (b) Simulations with varied exposure times. The width of the correlation window is 24 pixels.

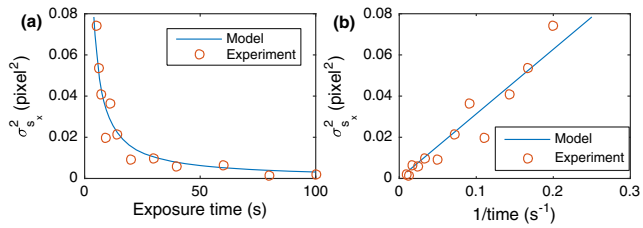


**Fig. 3.** Variance of the displacement (in pixels) in the x-direction for different exposure times in experiments. The width of the correlation window is 24 pixels.

exposure times from 5 to 100 s. The measured results follow the trend of the analytical model, even under non-ideal experimental conditions, e.g., the speckle patterns are not entirely homogeneous so the gradients may vary between different areas.

The other factor that affects the noise in the result is $\int w g_x^2 \mathrm{d}^2 r$, or the window function if we assume stationary statistics for the speckle pattern. Different window functions can be applied, such as a hamming window [11]. With a 2D rectangular window function in this Letter, it is the width $a$ of the window that determines the integration result directly as $\sigma_{s_x}^2 \propto 1/a^2$. The effect of subset choosing is previously observed and investigated in simulations and experiments [17]. In Eq. (4), it is analytically derived, and experiments are repeated below to support the derivation, as shown in Fig. 4. The speckle images are acquired with 40 s of exposure time and the same other settings as the experiments in Fig. 3. Different window sizes are adopted for integration of $g_x$ in Fig. 4(a) and for applying the correlation analysis in Fig. 4(b), where the variance of the shift for different window sizes is obtained experimentally (circles) and analytically (solid line). The variance decreases when the window size increases but, for sufficient window sizes, the improvement is small. The optimal window size varies with the system parameters, and the analytical model helps with finding it.

As discussed above, a larger window size will always provide lower noise. However, other image quality measurements are not included in Eq. (4). Most importantly, the resolution is lowered for larger window sizes. Hence, for completeness, we simulate the resolution dependence on the window size, retrieving the contrast-to-noise ratio (CNR) for objects with different spatial frequencies.

The objects are simulated as sinusoidal gratings made of plastic (polyethylene terephthalate). Their periods and thicknesses are equal, ranging from 20 μm to 2 mm. Hence, the

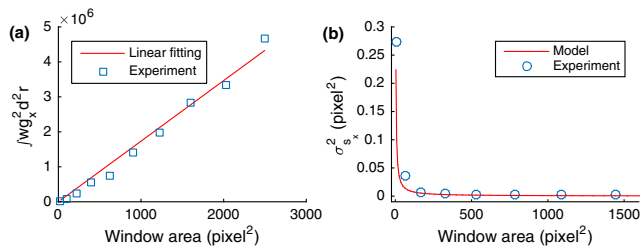


**Fig. 4.** (a) The denominator in Eq. (4) is linearly dependent on the window area $a^2$. (b) Variance of local shift when different window sizes are applied to the correlation analysis on the experimental images.

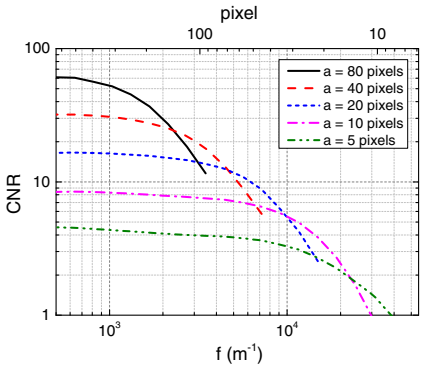


**Fig. 5.** CNR for objects with different spatial frequencies when varied window sizes are applied.

expected phase gradient is also of sinusoidal shape with the same amplitude for all objects. The simulations use a 1 m source-to-object and 2.9 m source-to-detector distance, leading to an effective pixel size of around 3.1 μm, and the spectrum from the liquid-metal-jet source. No obvious Talbot effect is observed, as the relatively large periods of the objects give long Talbot distances. Square windows $w$ with varied widths ($a = 5$, 10, 20, 40, and 80 pixels) are applied. The standard deviation of the noise is taken from experimental data with 5 min of exposure time and the same arrangement as for simulations. Under the assumption of white noise, the CNR is calculated as an image contrast divided by the standard deviation of the noise.

The results are shown in Fig. 5 for this particular application. The curves only continue until the contrast drops below 10%; as for lower contrasts, artifacts are most likely observed. As expected, the CNR for the objects of lower frequencies increases with window sizes, due to the lower noise levels. However, with increasing spatial frequency, the CNR drops faster for the larger windows due to the decrease in resolution. This illustrates the trade-off between the spatial resolution and noise in choosing the right window size.

In conclusion, an analytical model for noise assessment of the speckle-based differential phase contrast is proposed as Eq. (4). Some assumptions are necessary for this simplified model. (i) The sample image can be modeled as a displaced reference image, i.e., we assume a low-absorbing and smooth sample. (ii) The images have white Gaussian distributed photon noise. (iii) The speckle pattern has stationary statistics throughout the images, and the window size is large enough that the covariance of the gradients in two directions can be neglected as Eq. (5). (iv) The assessment error is small enough that we can omit the higher-order terms in the Taylor expansion in Eq. (3). (v) The image sampling is perfect, so the derivation does not need to include interpolations.

We expect to use this simple model as a reference in further optimization of SBI. Some parameters affecting the assessment error are discussed, namely quantum photon noise and window size. Increasing window size and increasing exposure time both lead to a reduction in the noise in the DPC image. We also show that for the single-shot speckle-tracking technique, the window size limits the spatial resolution. Using this model, we can predict the performance of the DPC signal from the speckle-based method, and make a balanced choice depending on window size and exposure time.

As can be seen from the model, the gradient of the speckle pattern, which is determined by the speckle size and contrast, also affects the DPC noise. We have not discussed it further, as it is affected by many parameters such as structure, material, and other properties of the diffuser, as well as the x-ray source, the detector, and the geometry of the arrangement. The ideal is a speckle pattern with large gradient, which means a small speckle size and a high contrast, while the pattern should not be periodic which can cause phase wrapping for larger phase shift. The diffuser should also not absorb too much of the flux. It might be difficult to find such a diffuser directly, as a smaller structure size of the random modulator normally generates lower-contrast speckle patterns.

This Letter focuses on the speckle-tracking technique. Other SBI techniques share essentially the same principle, but more restrictions are required for this simple model to be valid. For the speckle-scanning technique, the scan step needs to be larger than the effective pixel size, or the intensity patterns will be correlated to each other, and the white noise assumption in the derivation is no longer valid.

**Funding.** Knut och Alice Wallenbergs Stiftelse.

**Acknowledgment.** The authors thank Pierre Thibault and Simone Sala for fruitful discussions and Jakob Larsson and William Vågberg for assistance in the lab.

## REFERENCES

1. S. Berujon, E. Ziegler, R. Cerbino, and L. Peverini, Phys. Rev. Lett. **108**, 158102 (2012).
2. K. S. Morgan, D. M. Paganin, and K. K. W. Siu, Appl. Phys. Lett. **100**, 124102 (2012).
3. R. Cerbino, L. Peverini, M. A. C. Potenza, A. Robert, P. Bosecke, and M. Giglio, Nat. Phys. **4**, 238 (2008).
4. S. Berujon, H. C. Wang, and K. Sawhney, Phys. Rev. A **86**, 063813 (2012).
5. H. Wang, Y. Kashyap, and K. Sawhney, Sci. Rep. **6**, 20476 (2016).
6. T. Weitkamp, A. Diaz, C. David, F. Pfeiffer, M. Stampanoni, P. Cloetens, and E. Ziegler, Opt. Express **13**, 6296 (2005).
7. I. Zanette, T. Weitkamp, T. Donath, S. Rutishauser, and C. David, Phys. Rev. Lett. **105**, 248102 (2010).
8. T. Zhou, I. Zanette, M. C. Zdora, U. Lundstrom, D. H. Larsson, H. M. Hertz, F. Pfeiffer, and A. Burvall, Opt. Lett. **40**, 2822 (2015).
9. V. Revol, C. Kottler, R. Kaufmann, U. Straumann, and C. Urban, Rev. Sci. Instrum. **81**, 073709 (2010).
10. T. Zhou, U. Lundström, T. Thüring, S. Rutishauser, D. H. Larsson, M. Stampanoni, C. David, H. M. Hertz, and A. Burvall, Opt. Express **21**, 30183 (2013).
11. I. Zanette, T. Zhou, A. Burvall, U. Lundstrom, D. H. Larsson, M. Zdora, P. Thibault, F. Pfeiffer, and H. M. Hertz, Phys. Rev. Lett. **112**, 253903 (2014).
12. T. C. Chu, W. F. Ranson, M. A. Sutton, and W. H. Peters, Exp. Mech. **25**, 232 (1985).
13. L. N. Bohs and G. E. Trahey, IEEE Trans. Biomed. Eng. **38**, 280 (1991).
14. M. A. Sutton, S. R. Mcneill, J. S. Jang, and M. Babai, Opt. Eng. **27**, 870 (1988).
15. H. W. Schreier and M. A. Sutton, Exp. Mech. **42**, 303 (2002).
16. Y. Q. Wang, M. A. Sutton, H. A. Bruck, and H. W. Schreier, Strain **45**, 160 (2009).
17. B. Pan, H. Xie, Z. Wang, K. Qian, and Z. Wang, Opt. Express **16**, 7037 (2008).
18. D. M. Paganin, *Coherent X-Ray Optics* (Oxford University, 2009).
19. M.-C. Zdora, P. Thibault, F. Pfeiffer, and I. Zanette, J. Appl. Phys. **118**, 113105 (2015).